

Simplified modelling of photonic-crystal-confined vertical-cavity surface-emitting diode lasers

WŁODZIMIERZ NAKWASKI

Laboratory of Computer Physics, Institute of Physics, Technical University of Łódź,
ul. Wólczańska 219, 93-005 Łódź, Poland; e-mail: nakwaski@p.lodz.pl

In standard GaAs-based oxide-confined vertical-cavity surface-emitting diode lasers (VCSELs), their transverse single-fundamental-mode operation is limited to relatively low outputs. It is a direct consequence of small radial sizes of their active regions and strong real waveguiding effects induced by their oxide apertures. Photonic crystals applied in VCSEL designing in a way shown in the present paper enable a subtle waveguiding modification leading to a considerable increase in an output of the VCSEL single-mode operation. Unfortunately, the structure of a photonic crystal damages inside a VCSEL volume its axial symmetry, which makes rigorous simulation of its operation much more difficult. In the present paper, a simplified approach to physical (optical, electrical and thermal) phenomena taking place within VCSEL volumes equipped with photonic crystals is presented. Designing guidelines to obtain single-mode-operating photonic-crystal-confined VCSELs have been proposed. Various possible distributed-Bragg-reflector (DBR) output mirrors designed for various wavelengths have been analysed. From among them, GaN-based DBRs have been found to enable higher single-mode VCSEL outputs, especially for longer wavelengths.

Keywords: photonic crystals, vertical-cavity surface-emitting diode lasers (VCSELs), photonic-crystal -confined VCSELs, simplified VCSEL modelling.

1. Introduction

In many applications of vertical-cavity surface-emitting diode lasers (VCSELs), such as optical fibre communication and data recording on optical disks using optical methods, to name the most important ones, their single-fundamental-mode operation is required. In modern GaAs-based oxide-confined intracavity-contact VCSELs, this is usually accomplished by reducing the lateral size of their active regions [1]. In their too large active regions, excitation of higher-order transverse modes is favoured mostly because of strong current-crowding effect occurring close to the active-region edges [2]. Besides, a very low value of the refractive index of the oxide aperture, which means very strong radial index guiding, additionally enhances excitation of various modes. Therefore, the output of the single-fundamental-mode operation is in these devices limited to relatively low powers.

The oxide aperture is usually placed close to the anti-node position of the standing wave in the laser resonator, where the influence of the aperture on the optical wave is

the strongest. When this aperture is gradually shifted towards the node position of the standing wave, the strong radial index guiding of the aperture is steadily reduced. For its node position, the much weaker gain-guiding associated with a carrier distribution within the active region becomes a dominant waveguiding effect which enables an increase in the lateral active-region size, while the single-fundamental-mode operation is still preserved. It is, however, achieved at the expense of a considerably increased lasing threshold.

GaN-based VCSEL devices, on the other hand, suffer from a shortage of any efficient radial waveguiding mechanism analogous to oxide apertures in the above GaAs-based ones [3]. Therefore, until now, room-temperature (RT) continuous-wave (CW) operating GaN-based VCSELs have not been reported at all.

Photonic crystals (PCs) provide the modern technology of optoelectronics devices with a subtle method of an essential modification of optical material properties. In particular, some limitation (energy gap) in allowed energy (*i.e.*, wavelength) of propagated electromagnetic waves and/or anisotropic changes of material refractive indices may be created. Photonic crystals may also be used in VCSEL designing. A possible structure of such photonic-crystal-confined (PCC) VCSELs is presented in Sec. 2. The main goal of this paper is to propose a simplified modelling approach to PCC VCSEL designing.

2. Structure of the PCC VCSELs

There are many possible structures of PCC VCSELs. Two of them with electrical oxide apertures are shown in Fig. 1. Because of these apertures, they are the GaAs-based VCSELs. Confinement of current spreading may, however, be also achieved using high-resistivity lateral areas obtained, for example, with the proton-bombardment technique. So, generally, similar structures may be also produced without selective oxidation, which means that such PCC VCSELs may also be manufactured using GaN-based or InP-based structures.

A common feature of the PCC VCSELs proposed is the two-dimensional (2D) photonic crystal etched through a part of their output upper distributed-Bragg-reflector (DBR) mirrors. Because of some of its advantages [4], the structure of the triangular lattice of air columns is chosen. Such a photonic crystal is known to exhibit a complete band gap for all polarizations [4]. Unfortunately, it is not the case for light propagation along the direction perpendicular to the PC dielectric-constant periodic profile, as it is in the PCC VCSELs proposed for radiation travelling within their resonators between both DBR mirrors. However, it is possible in this case to take advantage of modification of averaged refractive indices by the PC structure.

As one can see in Fig. 1, the VCSEL radiation is proposed to be localized within the VCSEL cavity by the linear defect. Two possible defect structures are considered [5]:

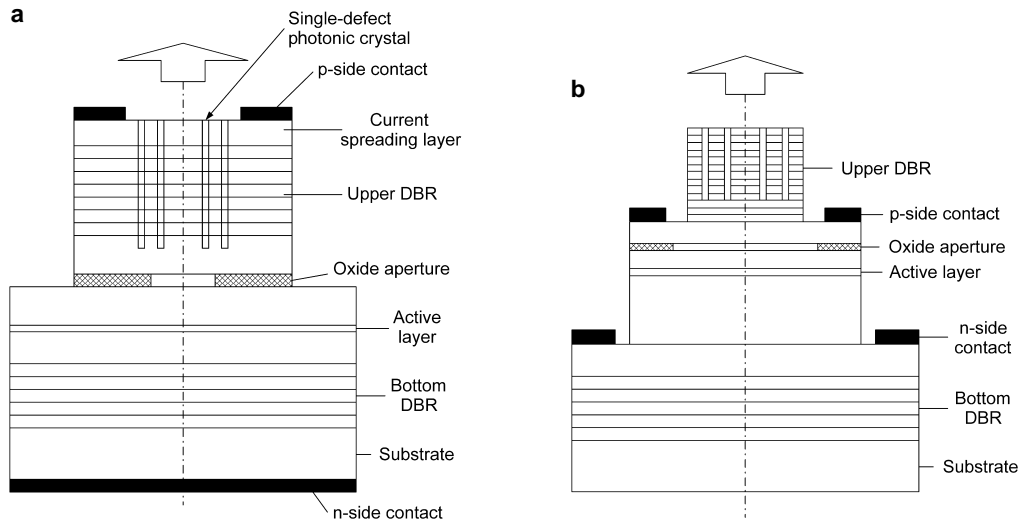


Fig. 1. Example structures of photonic-crystal-confined (PCC) GaAs-based VCSELs: a design with the annular upper contact deposited on the upper DBR structure (a), a design with two intracavity contacts (b).

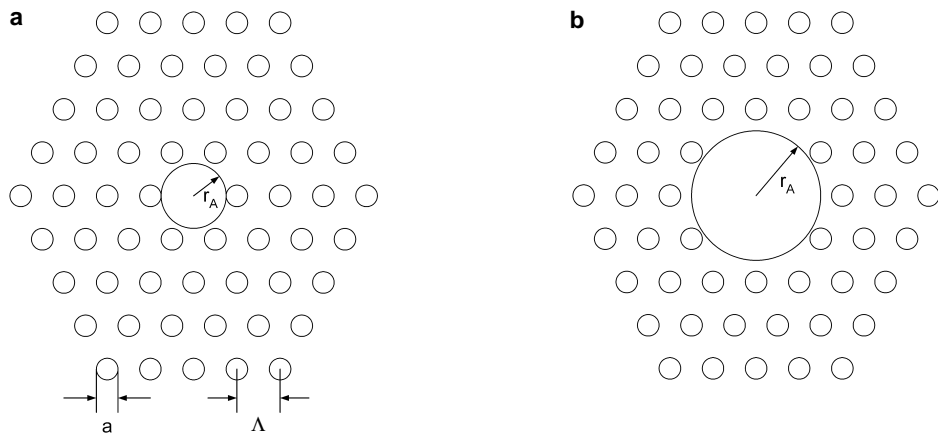


Fig. 2. Defect structure created within the two-dimensional triangle lattice of air columns by missing of: one air column (a), seven air columns (b).

- the single-point defect created simply by missing one air column of the photonic crystal etched through the upper DBR along the VCSEL axis (see Fig. 2a),
- the seven-point defect with seven missing air columns around this axis (Fig. 2b).

Then, in the centre of the VCSEL upper DBR, a uniform area of higher refractive index n_1 than the averaged index n_2 of surrounding area is created, which may be approximated by the step-index fibre. The radius r_A of the central higher-index fibre core may be expressed as

$$r_A = \begin{cases} \Lambda - \frac{a}{2} \\ \sqrt{3} \Lambda - \frac{a}{2} \end{cases} \quad (1)$$

where the first line corresponds to the single-point defect and the second one – to the seven-point defect and where (*c.f.* Fig. 2) Λ denotes the PC lattice constant. Then, depending on the hole diameter a , for the single-point defect structure, the radius r_A is within the following range:

$$\frac{\Lambda}{2} < r_A < \Lambda \quad (2)$$

whereas for the seven-point defect structure:

$$1.23\Lambda < r_A < 1.73\Lambda. \quad (3)$$

Rigorous modelling of an operation of PCC VCSELs is much more involved than in the case of traditional VCSELs because their cylindrical symmetry of all physical phenomena taking place within device volumes has been spoilt by PCs. Therefore, simplified simulation approaches are necessary to enable an approximate physical analysis of the performance of PCC VCSELs. In such an analysis, the VCSEL structure is divided into two assumed uniform areas [6], the central (core) one for $r < r_A$ and the cladding $r > r_A$ which enables preserving in this simplified simulation the cylindrical VCSEL symmetry. While values of physical parameters of the central area are unaffected by the PC, their effective values in the cladding area should be determined taking into account PC parameters Λ and a . Then the waveguide within the upper DBR part containing the PC structure may be approximated by the step-index fibre.

3. Radiation field in the step-index fibre

For the step-index fibre, with the refractive index equal to n_1 within the $r < r_A$ fibre core and to n_2 within the $r > r_A$ cladding:

$$n = \begin{cases} n_1 & r \leq r_A \\ n_2 & r \geq r_A \end{cases} \quad (4)$$

the numerical aperture (NA) of the fibre, expressing its light-gathering capacity, is given by (see Eq. (2.1.4) in [7]):

$$\text{NA} = n_1 \sqrt{2\Delta} \quad (5)$$

where Δ is the fractional index change of the core-cladding interface:

$$\Delta \equiv \frac{n_1 - n_2}{n_1}. \quad (6)$$

For the axially symmetric structures, the cylindrical (r, z, φ) co-ordinate system is the most convenient one. Then the general solution of Maxwell's equations contains six components of two vectors of the electric (\mathbf{E}) and the magnetic (\mathbf{H}) fields. Each of them is governed by the appropriate wave equation, but, for the system considered, only two of them are independent [8, 9]. It is customary to choose in this case the axial components E_z and H_z as the independent ones and to obtain the remaining ones in terms of them. Then the axial components may be expressed in the following form [7–9]:

$$E_z = \begin{cases} AJ_m(pr) \exp(im\varphi) \exp(i\beta z) & r \leq r_A \\ CK_m(qr) \exp(im\varphi) \exp(i\beta z) & r \geq r_A \end{cases}, \quad (7)$$

$$H_z = \begin{cases} BJ_m(pr) \exp(im\varphi) \exp(i\beta z) & r \leq r_A \\ DK_m(qr) \exp(im\varphi) \exp(i\beta z) & r \geq r_A \end{cases} \quad (8)$$

where A, B, C and D are constants whereas J_m and K_m are the Bessel functions of the first kind and the modified Bessel functions [10], respectively, and where

$$p^2 = n_1^2 k_0^2 - \beta^2, \quad (9)$$

$$q^2 = \beta^2 - n_2^2 k_0^2, \quad (10)$$

$k_0 = 2\pi/\lambda$ is the free-space wave number, β stands for the propagation constant and the azimuthal number m is restricted to take only integer values. For the $r < r_A$ core region, the remaining four field components may be expressed as follows [7]:

$$E_r = \frac{i}{p^2} \left(\beta \frac{\partial E_z}{\partial r} + \mu_0 \frac{\omega}{r} \frac{\partial H_z}{\partial \varphi} \right), \quad (11)$$

$$E_\varphi = \frac{i}{p^2} \left(\frac{\beta}{r} \frac{\partial E_z}{\partial \varphi} - \mu_0 \omega \frac{\partial H_z}{\partial r} \right), \quad (12)$$

$$H_r = \frac{i}{p^2} \left(\beta \frac{\partial H_z}{\partial r} - \epsilon_0 n^2 \frac{\omega}{r} \frac{\partial E_z}{\partial \varphi} \right), \quad (13)$$

$$H_\varphi = \frac{i}{p^2} \left(\frac{\beta}{r} \frac{\partial H_z}{\partial \varphi} - \epsilon_0 n^2 \omega \frac{\partial E_z}{\partial r} \right) \quad (14)$$

where ϵ_0 and μ_0 stand for the vacuum permittivity and the vacuum permeability, respectively, and $\omega = k_0 c$ is the optical field frequency. Analogous equations for the $r \geq r_A$ cladding area are obtained from Eqs. (11)–(14) after replacing p^2 by $-q^2$.

For each radiation mode, the A , B , C and D constants may be found assuming that the tangential components of \mathbf{E} and \mathbf{H} are continuous at the core-cladding boundary. The above leads to the following eigenvalue equation [7–9, 11]:

$$\left[\frac{J'_m(pr_A)}{pJ_m(pr_A)} + \frac{K'_m(qr_A)}{qK_m(qr_A)} \right] \left[\frac{J'_m(pr_A)}{pJ_m(pr_A)} + \frac{n_2^2}{n_1^2} \frac{K'_m(qr_A)}{qK_m(qr_A)} \right] = \frac{m^2}{r_A^2} \left(\frac{1}{p^2} + \frac{1}{q^2} \right) \left(\frac{1}{p^2} + \frac{n_2^2}{n_1^2 q^2} \right) \quad (15)$$

where primes indicate differentiation with respect to the argument.

The above eigenvalue Eq. (15) is used to determine allowed values of the propagation constant β . For each integer value of the azimuthal number m , multiple solutions may be possible. Therefore, their successive propagation constants are denoted as β_{mn} with $n = 1, 2, 3, \dots$. Then, for a given β_{mn} value, that is, for a given mode, spatial distributions of all 6 field components may be found from Eqs. (7)–(14). Those modes are denoted by HE_{mn} or EH_{mn} , depending on whether H_z or E_z dominates.

4. Single-mode VCSEL operation

Let us introduce the normalized frequency ν defined for the step-index fibre as [7, 11]:

$$\nu = r_A k_0 \text{NA}. \quad (16)$$

The normalized frequency, shortly, the parameter ν , determines the number of modes supported by the fibre: for large ν this number is approximately equal to $\nu^2/2$ [12].

The propagation constant β may be expressed as:

$$\beta = k_0 \left[bn_1 + (1 - b)n_2 \right] \quad (17)$$

where b is the normalized propagation constant, which may be approximately given using the formula [13]

$$b \approx \left(1.1428 - \frac{0.9960}{\nu} \right)^2 \quad (18)$$

which is accurate within 0.2% for $1.5 \leq \nu \leq 2.5$.

For weakly guided fibres, for which $\Delta \ll 1$, the axial components E_z and H_z (see Eqs. (7) and (8)) are relatively small. Then the HE_{11} fundamental mode becomes approximately linearly polarized and is often denoted as LP_{01} [14]. Then one of the transverse components can be taken as zero. Let us use the Cartesian co-ordinate system with the $0z$ axis directed along the propagation direction. Assuming $E_y = 0$, the E_x component of the LP_{01} mode is given by [13]:

$$E_x = E_0 \begin{cases} \frac{J_0(pr)}{J_0(pr_A)} \exp(i\beta z) & r \leq r_A \\ \frac{K_0(qr)}{K_0(qr_A)} \exp(i\beta z) & r \geq r_A \end{cases} \quad (19)$$

and the dominant magnetic field component is expressed as $H_y = n_2(\epsilon_0/\mu_0)^{1/2}E_x$. The above relation may be approximated by the Gaussian distribution of the following form:

$$E_x = A \exp\left(-\frac{r^2}{w^2}\right) \exp(i\beta z) \quad (20)$$

where w is called the effective spot radius. For $1.2 < \nu < 2.4$, it may be approximated within a 1% error by [15]:

$$\frac{w}{r_A} \approx 0.65 + 1.619\nu^{-3/2} + 2.879\nu^{-6}. \quad (21)$$

Then the effective core area is given by:

$$A_{\text{eff}} = \pi w^2 \quad (22)$$

and the core confinement factor Γ , determining the fraction of the mode power contained within the core, may be expressed as:

$$\Gamma \equiv \frac{\int_0^{r_A} |E_x|^2 r dr}{\int_0^{\infty} |E_x|^2 r dr} = 1 - \exp\left(-\frac{2r_A^2}{w^2}\right). \quad (23)$$

Telecommunication single-mode fibres are designed to operate for $2 < \nu < 2.4$, because, although Γ is quite high for $\nu = 2$ ($\Gamma(\nu=2) = 0.75$), it is dramatically reduced to only 0.20 for $\nu = 1$.

For the desired single-mode operation, when all modes except the HE_{11} fundamental one are cutoff, ν should be reduced below its critical value ν_{cr} [9]. The next two modes excited after the fundamental one are the HE_{01} and EH_{01} (called sometimes TE_{01} and TM_{01}) modes. For $m = 0$, the right-hand side of Eq. (15) is equal to zero, which is followed by [7]:

$$pJ_0(pr_A)K'_0(qr_A) + qJ'_0(pr_A)K_0(qr_A) = 0, \quad (24)$$

$$pn_2^2 J_0(pr_A)K'_0(qr_A) + qn_1^2 J'_0(pr_A)K_0(qr_A) = 0. \quad (25)$$

A guided mode decays exponentially within the cladding because (see Eq. (8)) $K_m(qr) \propto \exp(-qr)$ for $r \gg r_A$. Therefore the cutoff condition for the TE_{01} and TM_{01} modes may be simply expressed as: $q = 0$. Then, from Eq. (10): $\beta = n_2 k_0$ and from Eq. (9), taking into consideration Eqs. (5), (6) and (16):

$$pr_A = r_A k_0 \sqrt{n_1^2 - n_2^2} \approx r_A k_0 n_1 \sqrt{2\Delta} = r_A k_0 \text{NA} = \nu. \quad (26)$$

Then, from Eqs. (24), (25), the above cutoff condition for the HE_{01} and EH_{01} (*i.e.*, TE_{01} and TM_{01}) modes may be simply expressed as

$$J_0(\nu_{\text{cr}}) = 0 \quad (27)$$

or [10]

$$\nu_{\text{cr}} = 2.405. \quad (28)$$

Therefore, to design a single-mode fibre, its parameter ν should be lower than $\nu_{\text{cr}} = 2.405$. Taking into account Eqs. (5), (16) and (26), it corresponds to the maximal diameter D_{max} of the core area:

$$D_{\text{max}} \equiv \frac{\nu_{\text{cr}} \lambda}{\pi n_1 \sqrt{2\Delta}}. \quad (29)$$

There are many possible structures of PCC VCSELs. For the most popular ones, *i.e.*, VCSEL structures with GaN-based, GaAs-based or InP-based output DBR mirrors designed for 0.40- μm , 0.85- μm , 1.30- μm or 1.55- μm emission wavelengths, the maximal active-region diameters D_{max} for a single-fundamental-mode operation are plotted in Fig. 3 versus the fractional index change Δ (see Eq. (6)). The assumed estimated averaged values $n_{1, \text{av}}$ of the core area are listed in the Table. For each given

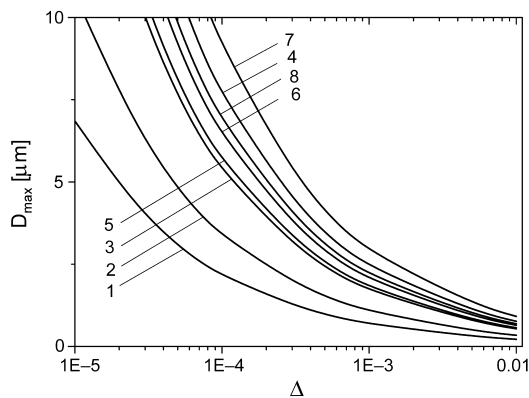


Fig. 3. Maximal active-region diameters D_{max} still ensuring the single-fundamental-mode operation in PCC VCSELs vs. the fractional index change Δ at the core/cladding interface plotted for various DBR mirrors and various emission wavelengths. Numbers of curves are defined in the Table.

T a b l e. Numerical data taken for determination of the parameter D_{\max} for various PCC VCSELs.

DBR number	DBR structure	λ [μm]	$n_{1, \text{av}}$
1	GaN-based	0.40	2.50
2	GaAs-based	0.85	3.40
3	GaAs-based	1.30	3.28
4	GaN-based	1.30	2.30
5	InP-based	1.30	3.10
6	GaAs-based	1.55	3.26
7	GaN-based	1.55	2.30
8	InP-based	1.55	3.05

DBR structure, an exact value of the above parameter should be determined for a given laser design using the detailed modelling of an optical field.

The fractional index change Δ depends on the PC parameters, *i.e.*, Λ and a , and on the depth of air columns [16]. It is evident from Fig. 3 that larger single-mode output (*i.e.*, larger values of the parameter D_{\max}) are obtained for lower Δ values. Besides, D_{\max} values are higher for low-index GaN-based DBRs than for GaAs-based or InP-based ones and for longer wavelengths. It is clearly confirmed that an application of a photonic crystal in VCSEL structures enables their careful modification to ensure higher-output single-mode operation, unachievable in standard VCSELs.

5. Simplified modelling of thermal and electrical phenomena

Similarly to the analysis of optical fields, analogous analyses of both the heat-flux and the current spreading phenomena within the PC VCSEL structure may be carried out assuming two areas, the core and the cladding, of different effective values of thermal and electrical parameters (Fig. 4). Besides, an anisotropy introduced by the PC structure, *i.e.*, different values of the above parameters in radial and axial directions, should be taken into account. For the thermal conductivity, its radial $k_{T,r}$ and axial $k_{T,z}$ components may be written as follows:

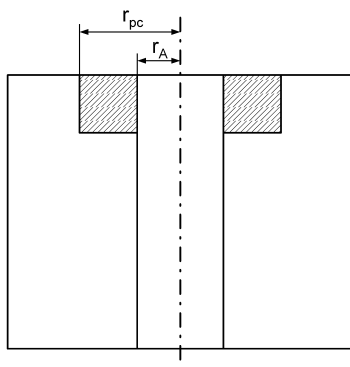


Fig. 4. Simplified thermal or electrical structure of PCC VCSELs (r_A and r_{pc} – internal and external radii of the photonic crystal structure).

$$k_{T,r} = k_T \Omega_r, \quad (30a)$$

$$k_{T,z} = k_T \Omega_z, \quad (30b)$$

whereas analogous ρ_r and ρ_z components of the electrical resistivity are expressed as:

$$\rho_r = \frac{\rho}{\Omega_r}, \quad (31a)$$

$$\rho_z = \frac{\rho}{\Omega_z} \quad (31b)$$

where

$$\Omega_r = 1 - \frac{a}{\Lambda}, \quad (32a)$$

$$\Omega_z = 1 - \frac{\pi}{4} \left(\frac{a}{\Lambda} \right)^2. \quad (32b)$$

For each structure layer, both its unaffected thermal conductivity k_T and electrical resistivity ρ for its core part are modified for its cladding part by the PC in a way shown in Eqs. (30)–(32).

6. Conclusions

In standard intra-cavity-contacted VCSEL structures, their single-fundamental-mode operation is practically limited to relatively low outputs, especially in oxide-confined ones. A careful application of PCs in their structures in a way shown in the present paper enables an increase in this important performance parameter. Higher achievable values of the single-mode output are found to be possible in VCSELs with GaN-based output DBR mirrors for larger wavelengths.

Many structures of VCSELs with photonic crystals are possible, because these crystals may be applied in various VCSEL areas, not only in their cavities. They seem to supply VCSEL designers with many new designing possibilities. Therefore, many new structures of VCSELs should be expected in the nearest future.

Acknowledgements – This work has been supported by the Polish State Committee for Scientific Research (KBN), grant 3-T11B-073-29 and 138/E-370/SPB/COST/P-03/DWM86/2004-2007 (COST P11 – Physics of linear, nonlinear and active photonic crystals).

References

- [1] SARZALA R.P., *A new approach to improve mode selectivity of higher output oxide-confined vertical-cavity surface-emitting lasers*, *Semiconductor Science and Technology* **19**(9), 2004, pp. 1122–4.

- [2] SARZAŁA R.P., MENDLA P., WASIAK M., MAĆKOWIAK P., BUGAJSKI M., NAKWASKI W., *Comprehensive self-consistent three-dimensional simulation of an operation of the GaAs-based oxide-confined 1.3- μm quantum-dot (InGa)As/GaAs vertical-cavity surface-emitting lasers*, *Optical and Quantum Electronics* **36**(4), 2004, pp. 331–47.
- [3] MAĆKOWIAK P., SARZAŁA R.P., WASIAK M., NAKWASKI W., *Radial optical confinement in nitride VCSELs*, *Journal of Physics D: Applied Physics* **36**(17), 2003, pp. 2041–5.
- [4] JOANNOPOULOS J.D., MEADE R.D., WINN J.N., *Photonic Crystals. Molding the Flow of Light*, Princeton University Press, Princeton, USA 1995, Chapter 5.
- [5] YOKOUCHI N., DANNER A.J., CHOQUETTE K.D., *Two-dimensional photonic crystal confined vertical-cavity surface-emitting lasers*, *IEEE Journal of Selected Topics in Quantum Electronics* **9**(5), 2003, pp. 1439–45.
- [6] ISTRATE E., SARGENT E.H., *Photonic crystal waveguide analysis using interface boundary conditions*, *IEEE Journal of Quantum Electronics* **41**(3), 2005, pp. 461–7.
- [7] AGRAWAL G.P., *Fiber-Optic Communication Systems*, Wiley-Interscience, New York, USA 2002.
- [8] MARCUSE D., *Light Transmission Optics*, Van Nostrand Reinhold Company, New York, USA 1972, Chapter 8.2.
- [9] MAURER R.D., Chapter 8 [In] *Introduction to Integrated Optics*, Barnoski M.K. [Ed.], Plenum Press, New York, USA 1974.
- [10] ABRAMOWITZ M., STEGUN I.A. [Eds.], *Handbook of Mathematical Functions with Formulas, Graphs, and Mathematical Tables*, Dover Publications, Inc., New York, USA 1972.
- [11] CHEO P.K., *Fiber Optics. Devices and Systems*, Prentice Hall, 1985.
- [12] GOWER J., *Optical Communication Systems*, Prentice Hall, London, Great Britain 1993.
- [13] JEUNHOMME L.B., *Single-Mode Fiber Optics*, Marcel Dekker, New York, USA 1990.
- [14] GLOGE D., *Weakly guiding fibers*, *Applied Optics* **10**(10), 1971, pp. 2252–8; *Dispersion in weakly guiding fibers*, *Applied Optics* **10**(10), 1971, pp. 2442–5.
- [15] MARCUSE D., *Gaussian approximation of the fundamental modes of graded-index fibers*, *Journal of the Optical Society of America* **68**(1), 1978, pp. 103–9.
- [16] YOKOUCHI N., DANNER A.J., CHOQUETTE K.D., *Etching depth dependence of the effective refractive index in two-dimensional photonic-crystal-patterned vertical-cavity surface-emitting laser structures*, *Applied Physics Letters* **82**(9), 2003, pp. 1344–6.

Received June 6, 2005